Evaluation of required connection load in GRS-IBS structures under service loads

F. Gebremariam[1], B. F. Tanyu[2], B. Christopher[3], D. Leshchinsky[4], J. G. Zornberg[5] and J. Han[6]

[1]*Graduate Research Assistant, George Mason University, Department of Civil, Environmental, and Infrastructure Engineering, VA, USA, E-mail: fgebrema@gmu.edu*
[2]*Associate Professor, George Mason University, Department of Civil, Environmental, and Infrastructure Engineering, VA, USA, E-mail: btanyu@gmu.edu (corresponding author)*
[3]*Geotechnical Consultant, Roswell, GA, USA, E-mail: barryc325@aol.com*
[4]*Adama Engineering and Professor Emeritus, University of Delaware, Clackamas, OR, USA, E-mail: adama@geoprograms.com*
[5]*Professor, The University of Texas at Austin, Department of Civil, Architectural, and Environmental Engineering, Austin, TX, USA, E-mail: jiehan@ku.edu*
[6]*Professor, The University of Kansas, Department of Civil, Environmental, and Architectural Engineering, KS, USA, E-mail: zornberg@mail.utexas.edu*

Received 06 January 2020, revised 06 April 2020, accepted 28 April 2020, published 19 October 2020

ABSTRACT: This study presents an evaluation of the connection load (T_o) and stress-strain conditions right behind the facing of a Geosynthetic Reinforced Soil – Integrated Bridge Structure (GRS-IBS) based on field instrumentation data obtained from an abutment constructed in Virginia. The observations from this site are compared against other projects in Delaware and Louisiana. The lateral stress distribution obtained from the field was observed to be lower than the active lateral earth pressure distribution but higher than predicted using the bin pressure method. The results from all sites showed that the reinforcement strains measured in the field were below the maximum geosynthetic strains allowed in the design of GRS-IBS. The distributions of both lateral stresses and reinforcement strains with depth were found to be approximately uniform. The T_o values for the Virginia structure were obtained based both on reinforcement strain and lateral stress data, which agreed well with each other. All sites indicated the existence of lateral stresses behind the facing, which contributed to the development of T_o. The normalized T_o values for all GRS-IBS projects evaluated in this study showed that the theoretical tributary area approach outlined in MSE design can be conservatively adopted to predict T_o in the design of GRS-IBS.

KEYWORDS: Geosynthetics, Geosynthetic reinforced soil (GRS), Integrated bridge system (IBS), Mechanically stabilized earth (MSE), Field monitoring program, Lateral stresses, Reinforcement strains, Connection load, Vertical and lateral deformations

REFERENCE: Gebremariam, F., Tanyu, B. F., Christopher, B., Leshchinsky, D., Zornberg, J. G. and Han, J. (2020). Evaluation of required connection load in GRS-IBS structures under service loads. *Geosynthetics International*, **27**, No. 6, 620–634. [https://doi.org/10.1680/jgein.20.00022]

1. INTRODUCTION

Mechanically stabilized earth (MSE) structures are composed of alternating layers of compacted high-quality granular backfill material reinforced with metallic or geosynthetic reinforcements. They have been used for the past several decades to support bridge abutments (Berg *et al*. 2009). In recent years, the Federal Highway Administration (FHWA) has been promoting an approach based on using only geosynthetics (primarily geotextiles and occasionally geogrids) to reinforce soil (granular backfill) to construct bridge abutments. This approach blends the bridge superstructure (bridge slab) with the integrated approach (roadway) through a jointless connection aiming to prevent the bump that may occur on the surface of the road at the end of bridges supported on deep foundations. This construction approach is referred to in the literature as a Geosynthetic Reinforced Soil (GRS) – Integrated Bridge System (IBS), also abbreviated as GRS-IBS (Adams *et al*. 2011; Adams and Nicks 2018). An important difference between MSE and GRS-IBS is the limits established for maximum vertical reinforcement spacing. According to the American Association of State Highway and Transportation

Officials (AASHTO), the vertical reinforcement spacing in MSE is limited to 0.8 m, whereas in GRS-IBS the spacing is limited to 0.3 m. Another difference is the connection of the reinforcements to the facing of the structure. In an MSE structure, both metallic and geosynthetic reinforcements may be mechanically or frictionally connected to the facing. However, in a GRS-IBS, the reinforcement is connected to the facing only through friction.

The design guidelines for the internal stability of MSE structures is based on the 'simplified method', which involves evaluation of the pullout resistance and connection strength (Berg *et al.* 2009). The lateral earth pressure is estimated using the classical lateral earth pressure distribution using Rankine's theory. Instead, the internal stability design of GRS-IBS is based on empirical relationships developed from the results of mini-pier tests conducted at the FHWA's Turner Fairbank Highway Research Center (TFHRC) (Adams *et al.* 2011; Adams and Nicks 2018). The internal stability analysis evaluates the ultimate capacity, deformations and required reinforcement strength with the details of the structure specifically prescribed. These include a height limited to 9 m, an allowable bearing pressure limited to 190 kPa, and lateral and vertical strains limited to 1% and 0.5%, respectively. The reinforced fill, type and strength of reinforcement, and reinforcement spacing are also restricted to a much tighter range than MSE walls. The lateral earth pressure is calculated based on a theoretical bin pressure concept, in which the pressure is assumed to be zero at the elevation of each reinforcement layer and the lateral pressure is considered a function of the reinforcement spacing rather than the height of the abutment (Wu 2001; Adams *et al.* 2011; Adams and Nicks 2018). Because GRS-IBS is considered a composite structure, the geosynthetic is assumed to deform laterally with the soil and the geosynthetic pullout capacity is not evaluated (Adams *et al.* 2011; Adams and Nicks 2018).

Awad and Tanyu (2014) conducted direct shear and pullout tests to investigate the governing mechanism of a frictionally connected MSE facing and determined that under normal loads, the sliding of blocks over a geotextile governs as failure mode over the pullout of a geotextile placed between the blocks. They also observed that the peak connection strength in direct shear is reached before the actual geosynthetic strength, which is not the case in pullout mode, implying that failure in a frictional connection could be more critical than if pullout would govern. The required connection strength in MSE is designed as the maximum tensile force in the reinforcement (Berg *et al.* 2009). In contrast, the assumption in GRS-IBS is that it is internally supported by closely spaced reinforcements and that the lateral stresses acting on the facing blocks are small; thus, the facing element is not considered a structural component except for providing a frictional connection. Consequently, an evaluation of connection strength is not required in the design of GRS-IBS (Adams *et al.* 2011; Nicks *et al.* 2013; Adams and Nicks 2018).

To investigate the relevance of connection loads and understand the stress-strain conditions immediately behind the facing in GRS-IBS structures, a literature review was conducted as part of this research to identify geosynthetic reinforced soil structures that served as bridge abutments, retaining walls, or experimental test structures, the performances of which have been monitored through instrumentation. Experimental tests were conducted to study the behavior of the structures to predict GRS performance in the field in which they were built, either as bridge abutments or retaining walls. The lateral earth pressures in full-scale MSE test walls has been generally reported to increase with depth, but the magnitudes of the measured pressures were less than the calculated pressures for active conditions (e.g. Christopher 1993; Morrison *et al.* 2006). However, Jiang *et al.* (2015) established that the lateral stress distribution with depth was uniform in an MSE wall with secondary reinforcements. Monitoring results from MSE abutments and full-scale MSE test walls in previous studies (Christopher 1993; Ling and Leshchinsky 1996; Allen and Bathurst 2002; Abu-Hejleh *et al.* 2003; Bathurst *et al.* 2005; Stulgis 2006; and Morrison *et al.* 2006), have indicated maximum vertical and lateral deformations in the reinforced mass below 35 mm and maximum geosynthetic strains less than 2%. Monitoring results from a load-carrying MSE abutment by Abu-Hejleh *et al.* (2003) confirmed that the location of the locus of the maximum geosynthetic tensile loads extended to the back edge of the footing, as originally recommended by Christopher *et al.* (1989) and currently recommended by FHWA (Berg *et al.* 2009) and AASHTO (2020). Allen and Bathurst (2002) reported that reinforcement loads in MSE walls could be estimated using geosynthetic reinforcement strains measured in the field under working stress conditions and the modulus of the geosynthetic reinforcement. Allen and Bathurst (2015, 2018) demonstrated that the 'simplified method' adopted in design of MSE structures does not provide accurate prediction of reinforcement loads and strains. The authors proposed an alternative approach referred to as the 'simplified stiffness method' to predict reinforcement loads in internal stability evaluation. The proposed method modifies the simplified method by considering the contribution of the reinforcement stiffness, the distribution of reinforcement loads, the facing stiffness and batter, and the cohesion of backfill in the estimation of reinforcement loads. The distribution of reinforcement loads with depth predicted by the proposed method follows a bi-linear distribution, not a triangular distribution as predicted by the simplified method. Most previous research involving field monitoring of GRS-IBS (Wu *et al.* 2001; Adams *et al.* 2011; Bloser *et al.* 2012; Budge *et al.* 2014; Warren *et al.* 2014; Adams and Nicks 2018) has focused on measuring settlement of the bridge and lateral deformation of the facing of the structure. The maximum settlement and lateral deformations observed from these studies were found to be less than 25 mm. Saghebfar *et al.* (2016) observed that the lateral earth pressures behind facing blocks of a GRS-IBS abutment were less than the theoretically calculated pressures for active conditions, and geosynthetic strain measurements showed that the locus of the slip surface did not match the theoretical failure line at a $45 + \phi/2$ inclination when surcharge loads were applied on the GRS-IBS abutment. Nicks and Adams (2019)

conducted experimental tests on GRS-IBS 'mini-abutments' and determined that the lateral earth pressure distribution in the field agreed with the theoretical stress distribution considering surcharge. However, the lateral earth pressure distribution under self-weight was observed to be comparatively uniform, which is inconsistent with the theoretically assumed triangular distribution. A recent numerical study (Ardah *et al.* 2018) conducted to evaluate the effect of differential settlement below the reinforced soil foundation (RSF), reinforced zone, and retained soil on the performance of GRS-IBS showed that the differential settlements have a major effect on the reinforcement strain distribution profile and facing lateral displacement, but have a comparatively minor effect on the lateral pressures acting on the facing.

The information gathered in the technical literature reveals that the stress-strain conditions right behind the facing in GRS-IBS structures have not been studied in detail. The required connection strength in GRS-IBS structures has also not been investigated thoroughly to date. Furthermore, in MSE structures (i.e. structures often constructed with the same backfill, reinforcement, vertical reinforcement spacing, facing, and reinforcement connection to the facing as in GRS-IBS), the design connection strength is adopted as the reinforcement maximum tension, whereas in GRS-IBS the connection strength requirement is not evaluated in the design. The research presented in this paper focuses on a field monitoring approach developed to investigate the required connection load in GRS-IBS structures based on field instrumentation data obtained from GRS-IBS built in Virginia as well as on data from other field monitored GRS-IBS projects in the U.S. It corresponds to the field component of a comprehensive evaluation of the effect of vertical spacing on the design of geosynthetic-reinforced soil structures (Zornberg *et al.* 2018, 2019). Primary focus is on stress and strain measurements collected through field monitoring data suitable to predict connection loads. Additionally, observations on the short-term and long-term performance of GRS-IBS structures related to foundation settlement and facing lateral displacement are presented in the paper.

2. CHARACTERISTICS OF THE VIRGINIA GRS-IBS

The GRS-IBS construction site where the field monitoring program was implemented is located on route 720 in Harrisonburg, Virginia. The GRS-IBS was built in a local farm area to replace an existing culvert used to allow the passage of water in an area that is classified as a seasonal dry streambed. The construction site is owned by the Virginia Department of Transportation (VDOT) and construction was conducted between 1 August and 15 September 2015 using VDOT in-house resources. The design of the GRS-IBS followed the design guidelines specified in the *Geosynthetic reinforced soil integrated bridge system interim implementation guide* (Adams *et al.* 2011; Adams and Nicks 2018).

The constructed GRS-IBS measures 2.2 m in height, 9 m in width and has a bridge span of 3.6 m that accommodates two-lane traffic access (Gebremariam *et al.* 2020). The GRS-IBS abutment was constructed using AASHTO No. 8 aggregate and a woven geotextile reinforcement with primary reinforcement spacing of 0.2 m and secondary reinforcement spacing of 0.1 m in the bearing bed zone. The GRS-IBS abutment has 16 geotextile layers including five secondary reinforcement layers placed in the bearing bed zone. The reinforced soil foundation (RSF) was constructed using VDOT 21B aggregate encapsulated by a woven geotextile. The thickness of the RSF is 0.7 m and it contains an additional reinforcement in its middle section. The facing of the abutment was constructed using standard concrete masonry unit (CMU) blocks that have a width and height of 0.2 m and a length of 0.4 m. Solid CMU blocks were used in the first four layers and split face CMU blocks were used in the remaining layers of the abutment. A segmented precast concrete slab was used to construct the bridge superstructure, while the integrated approach was constructed with the same materials used for construction of the RSF. The beam seat, where the bridge slab rests on the abutment, has a width of 0.6 m and the setback distance behind the facing blocks is 0.2 m.

A geotechnical site investigation and laboratory tests were conducted to identify subsurface stratigraphy and evaluate the properties of materials underlying the site. The results revealed that the foundation soils on which the new GRS-IBS abutment would rest are characterized primarily as an exposed limestone bedrock with pockets of residual stiff clay. The clay classifies as a CH material with a liquid limit of 72 and plasticity index of 45. No groundwater was encountered during the geotechnical site investigation.

According to the Unified Soil Classification System (USCS), the AAHSTO No. 8 aggregate used as the reinforced fill classifies as a poorly graded gravel (GP) with zero fines content. The aggregate had a maximum particle size of 12.5 mm and a density of 1.6 g/cm^3 (corresponding to a unit weight of 16.5 kN/m^3). The material's dry density during construction in the field was consistent with its maximum dry density. Based on the results of triaxial tests, the friction angle of the aggregate was 47.6°. The 21B aggregate used to construct the RSF had a maximum dry density of 2.2 g/cm^3 (corresponding to a unit weight of 22 kN/m^3) and optimum moisture content of approximately 8%. The dry density of the material reported in the field was consistent with the maximum dry density. The friction angle of the 21B aggregate was determined as 40°. The woven geotextile used for reinforcement had an ultimate tensile strength of 70 kN/m, as reported by the manufacturer.

3. FIELD MONITORING PROGRAM

The main purpose of the field monitoring program was to evaluate the stress-strain behavior within the main body of the GRS-IBS structure and immediately behind the facing

of the structure. To achieve this objective, lateral stresses behind the facing, lateral strains in the reinforcement immediately behind the facing, vertical deformation (settlement) beneath the foundation and lateral movements of the facing were monitored. Figure 1 shows instrumentation layout in the middle section of the abutment.

Lateral stresses behind the facing of the GRS-IBS abutment were monitored with rectangular pressure cells (RPCs). Each RPC involved a hydraulic pressure pad, a pressure sensor and an electric transducer. The RPCs in this project were custom designed instruments to fit the dimensions of the facing blocks with a measuring pressure ranging from 0 to 100 kPa. Figure 2a shows installation of a 0.2 m by 0.4 m RPC on a CMU block in the primary reinforcement zone, and a 0.1 m by 0.4 m RPC on a CMU block in the bearing bed zone.

Lateral strains in the reinforcement were monitored by foil strain gages (SG) that were characterized by a length of 50 mm long and a resistance of 120 Ω. The SGs were glued to the geotextile using an epoxy-type adhesive. Selection of the appropriate adhesive was determined after conducting wide-width strip tensile tests (ASTM D4595) in which the SGs were glued onto the geotextile specimens using both epoxy and silicon adhesives. Relationships between applied loads and the corresponding strains were developed from the test results. Both adhesive types used to glue the SGs onto the geotextile specimens provided similar strain levels for the same applied loads. However, because the silicon adhesive required a much longer curing time than the epoxy adhesive, use of epoxy was preferred. For redundancy, the SGs were designed for installation on both sides of the geotextile, with each pair placed at the same location. The SGs were installed prior to field construction on the actual geotextile to be used in the GRS-IBS and the geotextile was then placed at its proper location in the field. Silicon adhesive was applied on top of the SGs to protect them against damage by aggregate particles and water infiltration into the abutment. Figure 2b shows the location of the SGs as installed within the GRS abutment.

A settlement cell (SC) was placed underneath the RSF to monitor the overall vertical movement within the GRS. A conventional settlement plate could not be used, as it would have required a rod that penetrated both the RSF and the GRS-IBS. Therefore, the selected instrument operated via a system involving a vibrating wire, settlement cell pressure transducer, liquid-filled tubing, and reservoir. The instrument itself, where the pressure transducer is located, was mounted on a 0.3 m by 0.3 m steel plate and placed in a hole dug into the clay strata (Figure 2c). The liquid-filled tubing was then connected to the pressure transducer, which daylighted to the reservoir. The liquid used in the tubing contained a 50/50 mixture of water and ethylene glycol, which is approximately 7% heavier than water and does not freeze in winter seasons. The level of liquid in the tubing was maintained by adding liquid to the reservoir at regular intervals as recommended by the manufacturer. The reservoir was installed on stable ground at a comparatively high elevation outside the GRS abutments and data was collected from a readout box adjacent to the GRS-IBS.

Survey targets (ST) were used to monitor long-term movements of the facing of the structure. Targets were

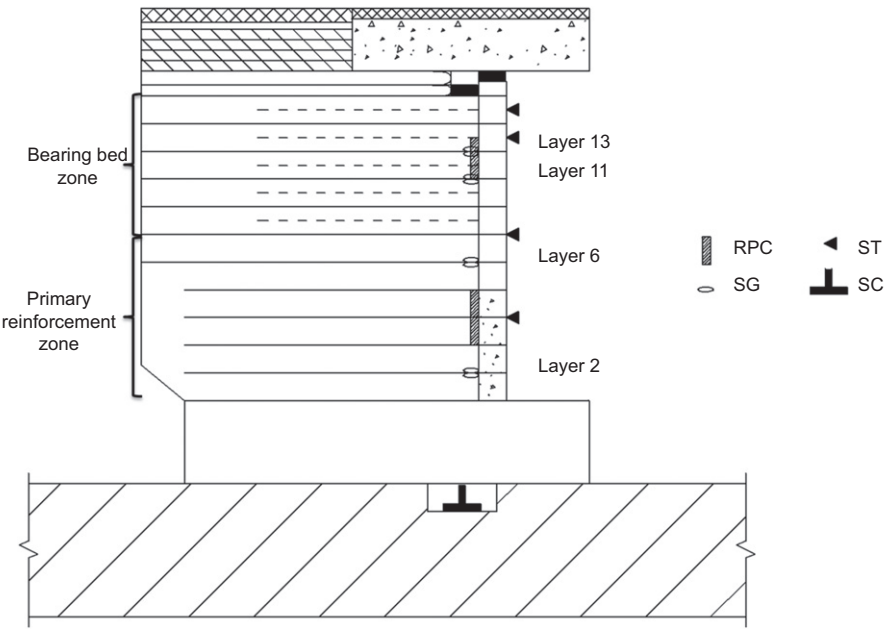

Vertical scale: Each rectangle shown on the figure along the facing of the abutment refers to 0.2 m high CMU block. There are total of 11 blocks, resulting in 2.2 m height.

Notes: RPC: Rectangular pressure cell, SG: strain gage, SC: settlement cell, and ST: survey target.

Figure 1. Instrumentation layout of GRS-IBS constructed in this study. Notes: RPC: Rectangular pressure cell, SG: strain gage, SC: settlement cell, and ST: survey target

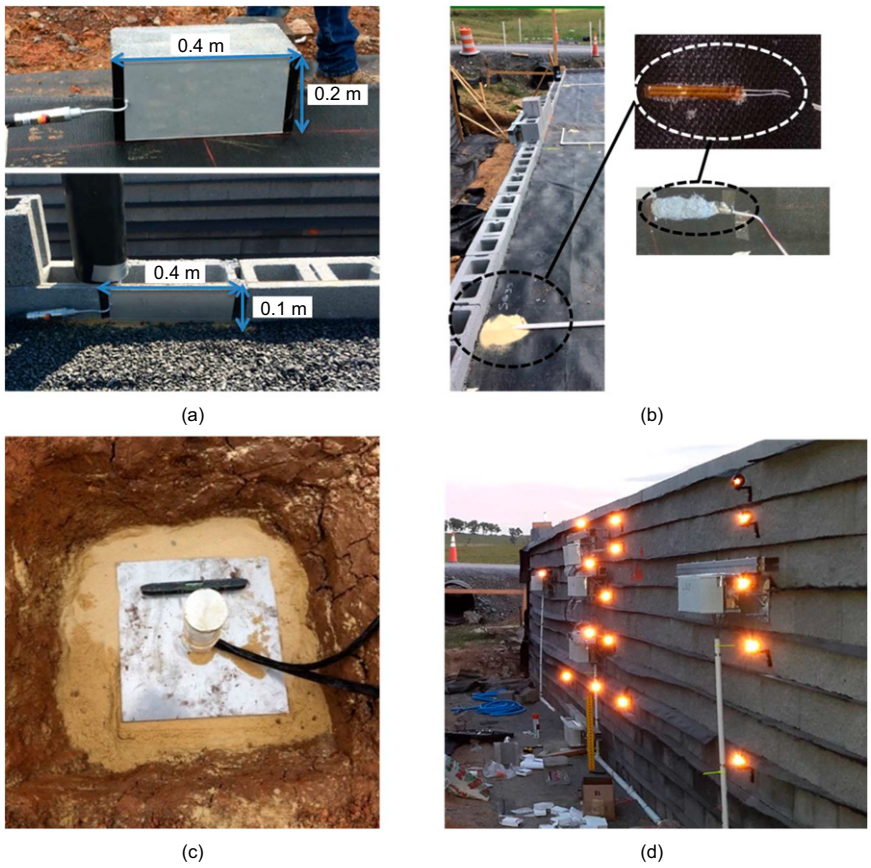

Figure 2. Instrument installation in GRS-IBS: (a) Rectangular earth pressure cells; (b) strain gages; (c) settlement cell; and (d) survey targets (illuminated)

surveyed right before and after placement of the bridge slab, and four times after construction, but surveying was not conducted during construction. The total station used for surveying had an accuracy of 1 mm in both lateral and vertical directions. Figure 2d shows the locations of the survey targets on the facing blocks of the GRS-IBS.

4. ASSESSMENT OF THE GRS-IBS GENERAL PERFORMANCE

The performance during construction of the Virginia GRS-IBS was assessed considering the increasing loads due to the backfill self-weight and placement of the bridge slab using data obtained from the installed instrumentation. Assessment of the GRS-IBS general performance focuses on evaluating the lateral stresses and reinforcement strains behind the facing blocks and vertical and lateral deformations of the structure. The subsequent sections present details of the observed behavior.

4.1. Lateral stress monitoring

The lateral stresses behind the facing blocks were monitored by RPCs installed in five layers of the abutment. Lateral stresses developed due to backfill self-weight during construction, as shown in Figure 3. The stress distribution profile obtained from field data is compared with the theoretical active and at-rest earth pressure distributions predicted using the properties, as follows (AASHTO 2020))

$$\sigma_{\mathrm{H}} = K\left((\gamma \times Z) + \Delta\sigma_{\mathrm{V}}\right) \tag{1}$$

where σ_{H} is the lateral earth pressure, γ is the unit weight of the backfill material, Z is the depth at a given stress point, and $\Delta\sigma_{\mathrm{V}}$ is the vertical stress distributed from the slab load.

The earth pressure coefficient, K, which is a function of the backfill friction angle (ϕ) is predicted as follows

$$K_{\mathrm{a}} = \tan^2\left(45 - \frac{\phi}{2}\right) \tag{2}$$

$$K_{\mathrm{o}} = 1 - \sin\phi \tag{3}$$

where K_{a} is the active lateral earth pressure coefficient (Rankine's theory for a wall with no sloping backfill) and K_{o} is the at-rest lateral earth pressure coefficient (Jaky, 1948).

Figure 3a presents a comparison between the lateral stress distribution with depth due to backfill self-weight as defined by field monitoring data and the lateral stress distributions computed from the theoretical methods discussed previously (Equations (1)–(3)). The lateral earth pressure distribution in current GRS-IBS design is estimated based on the bin pressure theory, where the lateral earth pressure is assumed to increase within a given layer and becomes zero at the next reinforcement layer (Wu 2001; Adams *et al.* 2011; Adams and Nicks 2018).

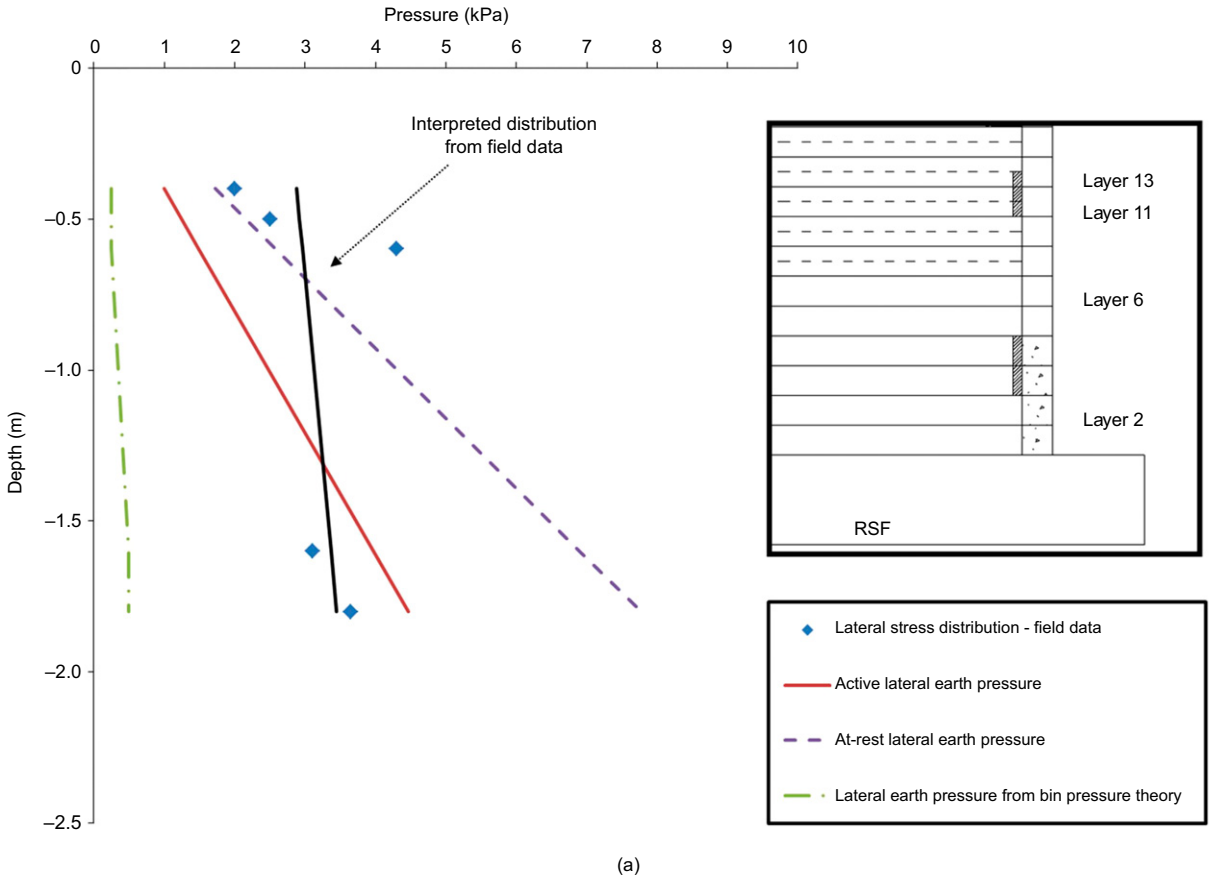

(a)

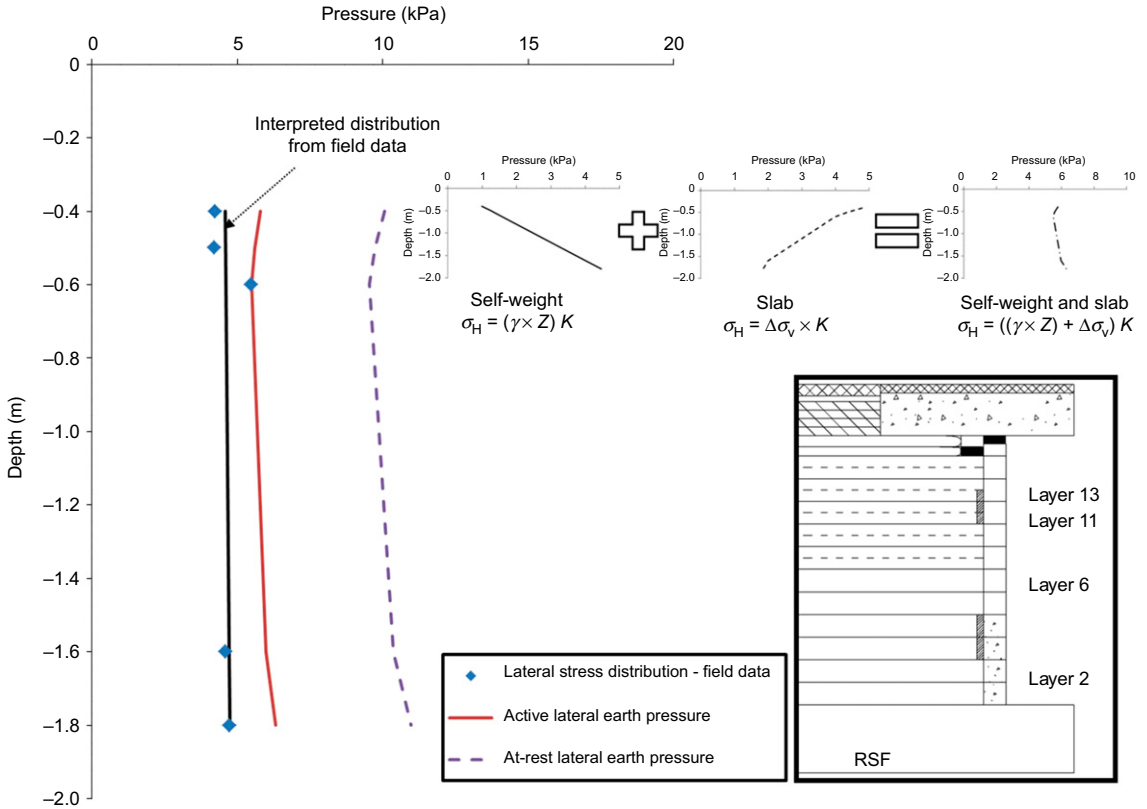

(b)

Figure 3. Lateral stress distribution obtained in the GRS-IBS constructed in this study and comparison of field data with theoretical calculations based on: (a) self-weight of backfill load; and (b) additional slab load

The lateral earth pressure predicted with this method is assumed to be a function of the vertical reinforcement spacing (S_v) and not a function of depth at a given stress point (Z). Figure 3a also depicts the lateral earth pressure with depth predicted using the bin pressure theory. The lateral pressure in the bin pressure method is calculated using Equation (1). However, instead of Z, computations are made using S_v. Comparison of the lateral stress from field data points shown in Figure 3a with the stress distributions predicted with the different earth pressure theories reveals that the lateral stress distribution obtained under self-weight conditions from the GRS-IBS constructed in this study does not show a triangular distribution, as adopted in the earth pressure theories, but rather follows a reasonably uniform trend. A uniform trend in the lateral stress distribution with depth due to self-weight is consistent with observations reported by Jiang *et al.* (2015) and Nicks and Adams (2019). Also, the trend defined by field data appears to be consistent with the stress distribution predicted using the bin pressure method, although the field stress magnitudes is significantly higher than the predicted values.

The lateral stress distribution profile, which results from adding the bridge slab loads to the existing self-weight loads, was also compared against the lateral stress distributions predicted from theoretical methods, as shown in Figure 3b. The insert in Figure 3b displays the steps followed to estimate the theoretical stress distributions that combine the effects of both self-weight and slab load in accordance with Equation (1). The vertical stress distributed from the slab load ($\Delta\sigma_V$) was calculated using the AASHTO 2 : 1 vertical stress distribution method (also known as the truncated 2 : 1 method, which considers the effect of wall facing on the stress distribution). The vertical stress distribution was calculated for all layers, in which the lateral stresses were measured in the field. The magnitude of the slab load was 42 kPa and the vertical stresses distributed from the slab at depths corresponding to the locations of the five RPCs were 31.8, 28.9, 26.6, 13.3, and 12.3 kPa, respectively. The data in Figure 3b indicate that with the placement of the slab, the lateral stress distribution in the field became more similar to that defined by the active condition. In general, the reasonably uniform trend followed by the lateral stress distribution after placement of the slab was similar to that observed after placement of the fill. When compared, the trends exhibited in Figures 3a and 3b show similar distributions with depth, although the magnitude of the stresses in Figure 3b (self-weight and slab loads) was higher than that observed in Figure 3a (self-weight loads), as expected.

4.2. Reinforcement strain monitoring

Reinforcement strains were measured by SGs installed within the geotextiles placed at four reinforcement layers within the abutment (Figure 1). Twenty-four SGs were installed immediately behind the facing blocks located in the middle, north and south sections of the abutment. Of the 24 SGs installed in the field, only 16 survived field installation to generate data. Table 1 shows the geotextile strains generated due to backfill self-weight and slab loads as measured by the SGs installed at different locations.

The strain data presented in Table 1 correspond to an average of the strain values obtained from SGs installed at a given point on the top and bottom of the geotextile layer in the middle, north, and south sections of the abutment. As the data in Table 1 indicate, the largest strain (0.15%) right behind the facing in the bearing bed zone was obtained from the strain gages located at the middle section of the abutment. The strains measured from the north and south sides showed comparatively smaller strains (0.1%). The disparity in strain measurements is believed to be due to experimental test loadings that occurred during construction in the middle section of the abutment. Comparatively higher strains (0.21%) were recorded in layer 6 by SGs located in the middle section compared to SGs located in the south section of the abutment. It is anticipated that locked-in strains also occurred in this layer due to staged loading conducted during construction operations. The maximum strain level recorded by SGs installed in the bearing bed zone was 0.15%. This decrease in strain level may have been due to the closely spaced reinforcement in this zone reducing the lateral deformations and/or because the SGs in this zone were not as affected by the test loadings as the SGs in the primary reinforcement zone. When comparing the data from all SGs located right behind the facing blocks, the strains from both bearing bed and primary reinforcement zones appear generally comparable, with the exception of slightly higher strains recorded in the primary

Table 1. Strains measured in GRS-IBS due to the placement of the slab

Layer	North		Middle		South		SW			SW+SL		
	SW ε (%)	SW+SL ε (%)	SW ε (%)	SW+SL ε (%)	SW ε (%)	SW+SL ε (%)	ε Min. (%)	ε Avg. (%)	ε Max (%)	ε Min. (%)	ε Avg. (%)	ε Max (%)
13	N/A	N/A	0.1	0.1	0.15	0.15	0.1	0.13	0.15	0.1	0.13	0.15
11	0.13	0.15	0.15	0.15	N/A	N/A	0.13	0.14	0.15	0.15	0.15	0.15
6	N/A	N/A	0.21	0.21	0.13	0.13	0.13	0.17	0.21	0.13	0.17	0.21
2	0.1	0.1	0.16	0.17	0.1	0.1	0.1	0.12	0.16	0.1	0.12	0.17

Note: SW: self-weight of backfill load, SW + SL: self-weight and slab loads, ε: geotextile strain measured in the field, N/A: strain data not available.

reinforcement zone. The strains measured during construction of the GRS abutment did not show much change after the bridge slab was placed. In all cases, the maximum strains obtained from the field (0.21%) were significantly below the maximum allowable geosynthetic strains in the design of abutments reinforced with geosynthetics (2%) (Adams *et al*. 2011; Adams and Nicks 2018).

Table 1 also shows minimum, average, and maximum strains measured by SGs installed in layers in the middle, north, and south sections of the abutment. These values were recorded to capture strain data that was not available in some layers (e.g. strain data from layers 6 and 13 in the north section) and determine the effect of the test loadings in generating higher strains in the middle section of the abutment. Figure 4 presents the minimum, average, and maximum reinforcement strain distributions with depth due to self-weight and slab loads. The strain distribution with depth depicted in Figure 4 can be interpreted as reasonably uniform. The uniformity of the reinforcement strain distribution immediately behind the facing blocks obtained from SG data was found to be similar to the uniform lateral stress distribution obtained from RPC data.

4.3. Deformation monitoring

Settlement of the GRS-IBS abutment foundation was monitored via a settlement cell installed below the RSF. The settlement measured during and after construction is displayed in Figure 5. The maximum foundation settlement observed right after construction of the GRS-IBS was less than 1 mm. Consequently, the overall conclusion drawn from this data is that no or negligible settlements developed within the soil below the abutment during construction. The maximum foundation settlement observed 2.5 years after construction was slightly less than 3 mm, which may be attributed to the soil below the reinforced soil having large pockets of exposed bedrock close to the surface (Figure 5).

Sixteen survey targets were mounted on the CMU blocks of the abutment to monitor the long-term movements of the structure's facing. Lateral displacements of the abutment facing after construction are shown in Figure 6. The data in Figure 6 were obtained from the survey targets installed in the middle (Figure 6a) and north (Figure 6b) sections of the abutment immediately following placement of the slab and four times after construction. The results show that there was a continuous outward deflection of the facing blocks, with the magnitude of the maximum recorded value being 4.5 mm. The increases observed in facing displacements were cumulative and caused by live loads after the GRS-IBS opened to traffic. Considering the accuracy of the surveying, the data show that the maximum movement of the facing blocks was observed in the top half section of the abutment and the movement close to the foundation was very small. Overall, the data obtained from the settlement cells and surveying revealed that the vertical and lateral deformations in the structure after construction were small and well within the 0.5% vertical strain and 1% lateral strain limits specified in the design of GRS-IBS (Adams *et al*. 2011; Adams and Nicks 2018).

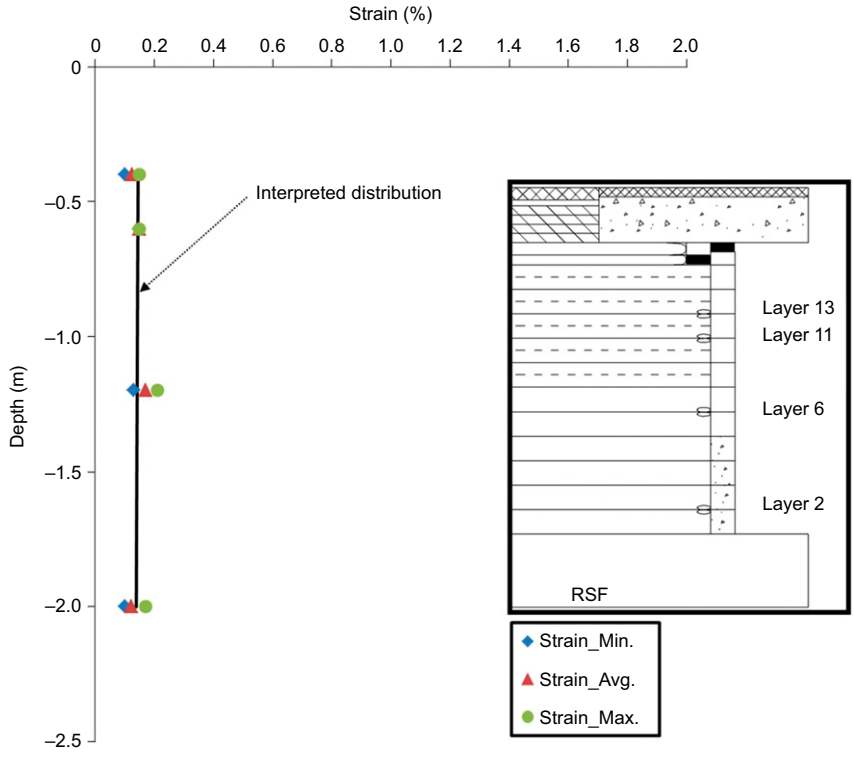

Note: The interpreted distribution was drawn based on the average strain data.

Figure 4. Reinforcement strain distribution with depth in GRS-IBS after placement of slab load

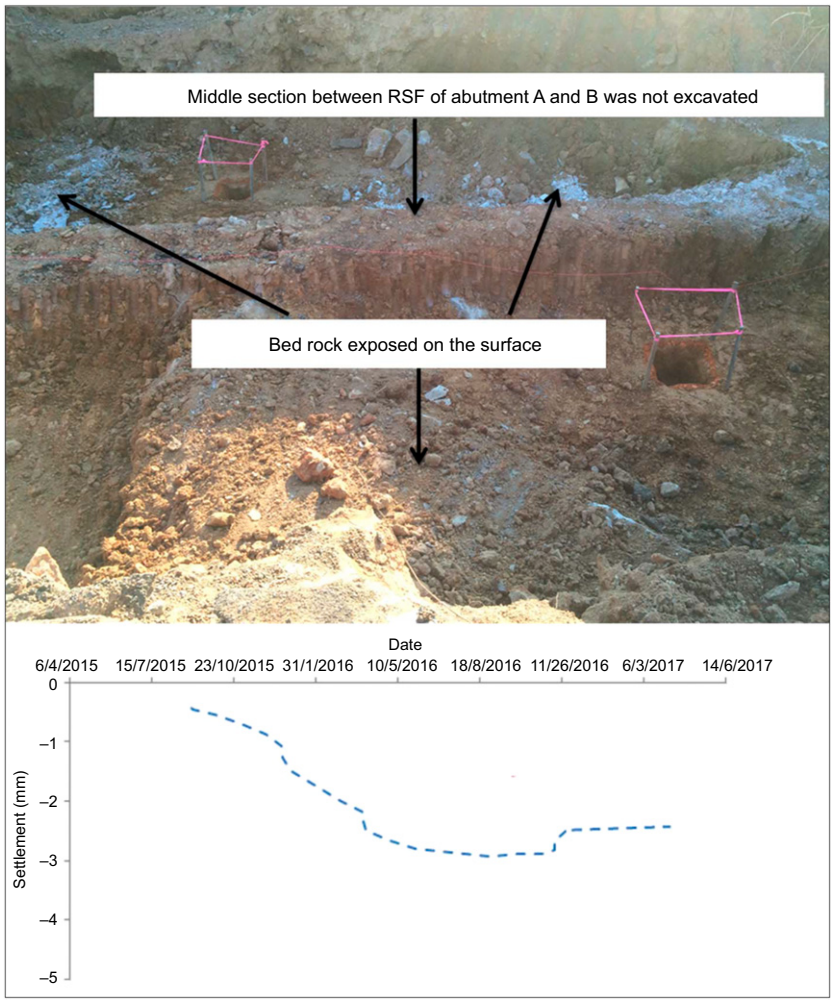

Figure 5. Settlement measured below the reinforced soil foundation of GRS-IBS

5. EVALUATION OF CONNECTION LOAD (T_O) IN GRS-IBS STRUCTURES

The data collected from the GRS-IBS constructed in this study provided an opportunity to evaluate the connection load (T_o) right at the facing to determine the magnitude and distribution with depth. This evaluation was conducted using two different approaches. In the first approach, T_o was estimated based on the strain data obtained from the SGs installed on the geotextile reinforcement right behind the facing, which is the most common method that has been used for this type of assessment. In the second approach, T_o was estimated based on the lateral stress data measured by RPCs mounted on the facing blocks. Observations from the two different approaches were compared and the overall observations were then compared to the T_o values obtained from other field-monitored GRS-IBS projects. The following sections provide details of these comparisons.

5.1. Estimating T_o as a function of reinforcement strain (Approach 1)

SGs were installed immediately behind the facing blocks (Figure 1) to facilitate evaluation of the load at the reinforcement-facing block connection that is expected to develop because of the lateral earth pressure acting on the facing blocks. Some load may also develop due to downdrag created by differential settlement between the reinforced fill and the block facing units. The load at the connection was estimated using the reinforcement strains measured by the SGs considering the modulus of the geotextile used as reinforcement. The relationship between the reinforcement load and strain is as follows

$$T_o = J \times \varepsilon \tag{4}$$

where T_o is the connection load, J is the stiffness of the geotextile, and ε is geotextile strain.

In this study, the stiffness of the geotextile at 2% strain was 700 kN/m, as reported by the manufacturer (Tencate Geosynthetics 2015). Additional laboratory tests were conducted following ASTM D4595 procedures, with results indicating that the average stiffness of the geotextile at a 2% strain level was approximately 700 kN/m. Consequently, the geotextile stiffness was considered as 700 kN/m for the purpose of estimating T_o. However, it should be noted that this modulus value was determined according to ASTM D4595, in which the geotextile sample is tested without the confinement of soil, which would potentially result in a modulus increase. Yet, such an increase may be somewhat offset by the rapid rate of

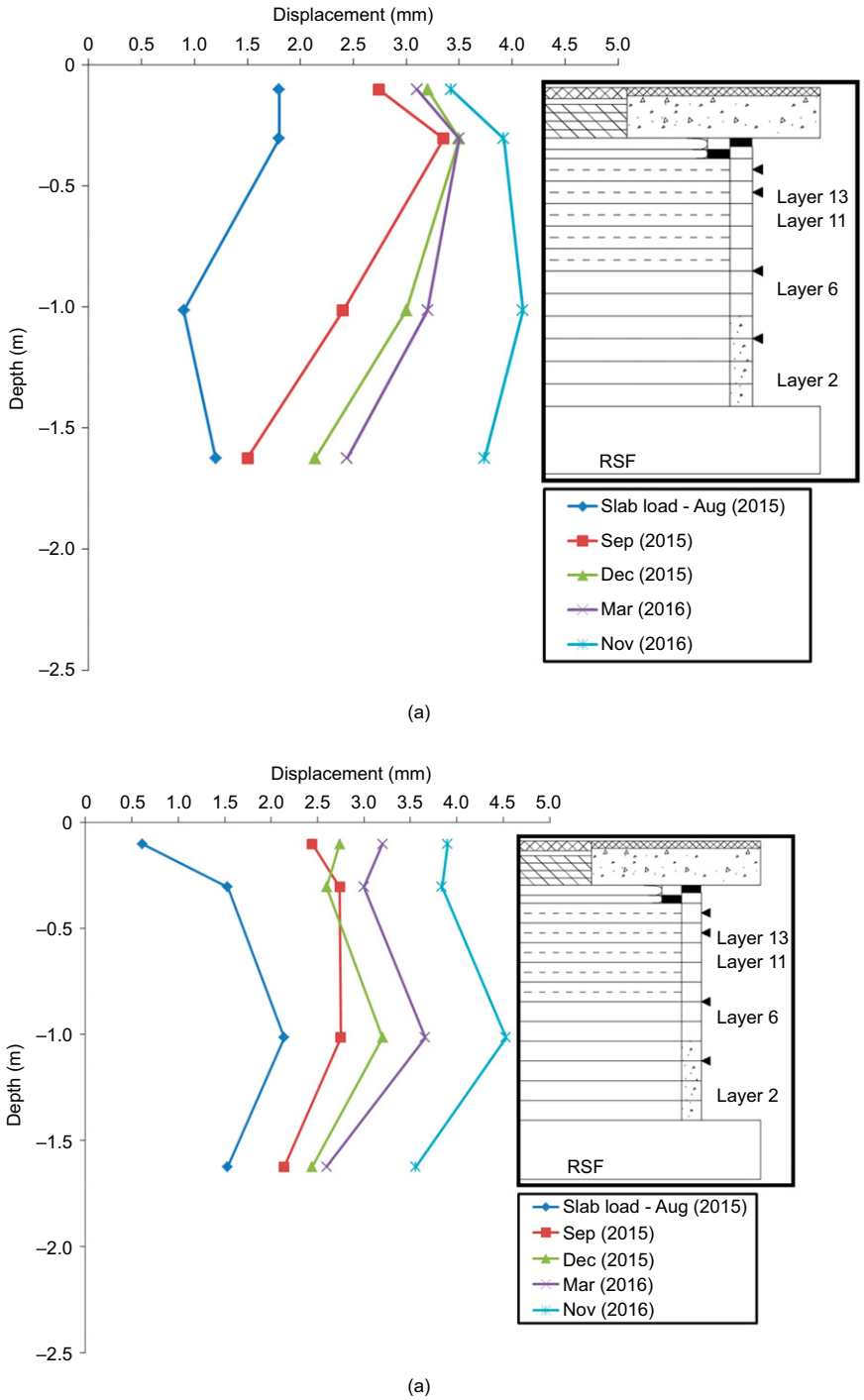

Figure 6. Lateral movements of facing blocks observed from survey targets installed on GRS-IBS: (a) middle section; and (b) north side of abutment. Note: The black triangles show in the inserts represent the location of the installed survey targets

testing used for the wide width test versus the rate of loading in the field, as demonstrated by Allen and Bathurst (2019). As a result, some uncertainty remains regarding the actual geotextile stiffness under field conditions.

Figure 7 shows the distribution of the calculated T_o based on Equation (4) (referred to herein as Approach 1) with depth. The depth values in this figure correspond to the locations of the SGs within the GRS-IBS. The strain values used in Equation (4) were the average strains measured by the SGs installed in the middle, north and south sections of the given depth within the abutment. The T_o values based on self-weight were calculated from the strains measured at the end of construction (before placement of the slab). The T_o values calculated to represent post-construction conditions were determined from the cumulative strains (combining the effects of self-weight of the backfill and slab load) recorded after placement of slab. The data show that placement of the slab led to a slight increase in T_o and the overall trend observed from the self-weight condition was very similar to that observed after placement of the slab. The

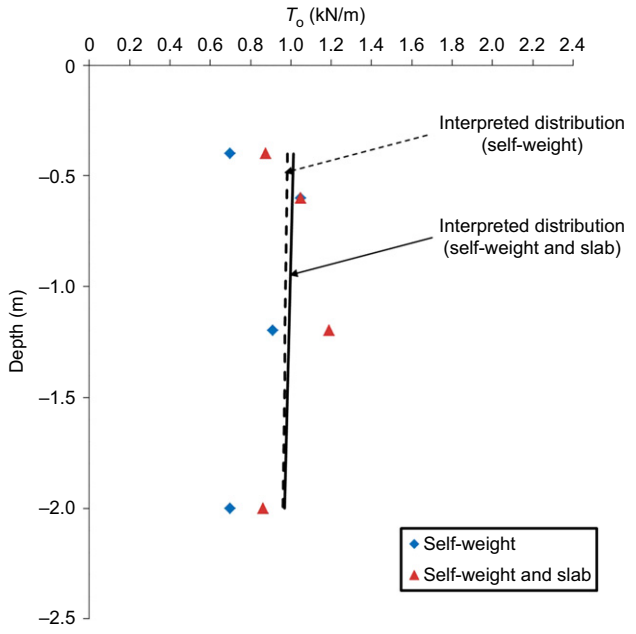

Figure 7. Connection load (T_o) distribution of GRS-IBS as determined from strain gages

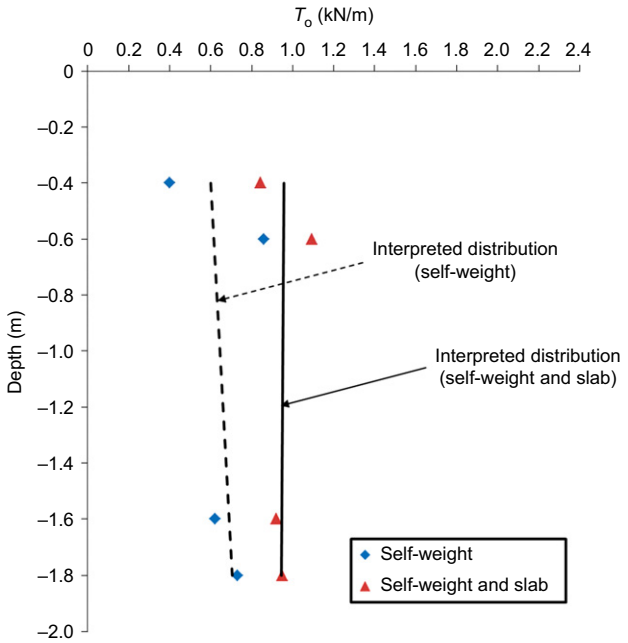

Figure 8. Connection load (T_o) distribution of GRS-IBS as determined from rectangular earth pressure cells

magnitude of the T_o after placement of the slab ranged between 0.8 and 1.2 kN/m, with the highest value measured at the mid-height of the abutment. With the exception of the data point at mid-height, the distribution of T_o with depth is considered fairly uniform. Based on this observation and the very small difference between the calculated T_o values, the overall distribution of T_o with depth is considered reasonably uniform, as shown in Figure 7.

5.2. Estimating T_o as a function of lateral stress (Approach 2)

The internal stability evaluation of MSE structures based on the simplified method (Berg *et al.* 2009) requires the connection strength between the reinforcement and facing of the structure to be designed to withstand maximum tension within the reinforcement (T_{max}). Based on this requirement, in Approach 2, the T_o values for the GRS-IBS constructed as part of this study were estimated as a function of the parameters used to estimate T_{max}, which is calculated as a function of the lateral earth pressure (σ_H) and the spacing between vertical reinforcements (S_v), as follows

$$T_{max} = \sigma_H \times S_v \quad (5)$$

Lateral stresses incorporated into Equation (5) were directly obtained from the RPCs at the back of the facing blocks. Although five RPCs were installed in this study, one RPC was installed in the bearing zone, where the geotextile reinforcement is deliberately not frictionally connected to the facing blocks. Consequently, the data from this RPC was not considered in this evaluation. As for the first approach, the estimated T_o values are presented with depth, which corresponds to the location of each RPC. Figure 8 shows the distribution of the calculated T_o values based on lateral stress measurements obtained at the end of construction (before placement of the slab) and cumulative stress values observed after placement of the slab. Similar to the strain data used in Approach 1, the RPCs showed an increase in magnitude after the slab was placed. The magnitude of the T_o values estimated based on the second approach also ranged from approximately 0.8 to 1.2 kN/m. As seen in Figure 8, the interpreted distribution of the T_o values after placement of the slab can also be considered to show a reasonably uniform trend with depth.

5.3. Comparison of T_o estimated using Approaches 1 and 2

Figure 9 compares the T_o profiles estimated using both approaches for the loading conditions existing before and after placement of the slab. The T_o values from the stress data were slightly lower than the strain data for self-weight load (Figure 9a). However, after the slab was placed, the magnitudes of T_o values estimated using both approaches were very close to one another (Figure 9b). This provides evidence of the adequacy of the behaviors observed from the strains measured in the reinforcements and lateral stresses collected at the back of the facing blocks. This good comparison is significant because, as noted earlier, the stiffness (J) of the geotextile used in Equation (4) did not correspond to values obtained from tests conducted under the confinement of soil and following field loading rates.

The scale at which the T_o values are plotted in Figure 9 suggests that the profile shows slightly lower values towards the top and bottom of the abutment, with some increase at roughly mid-height. However, considering the difference in magnitude of the T_o values, the overall distribution for each approach can still be considered, as indicated by the trend lines in Figures 7 and 8.

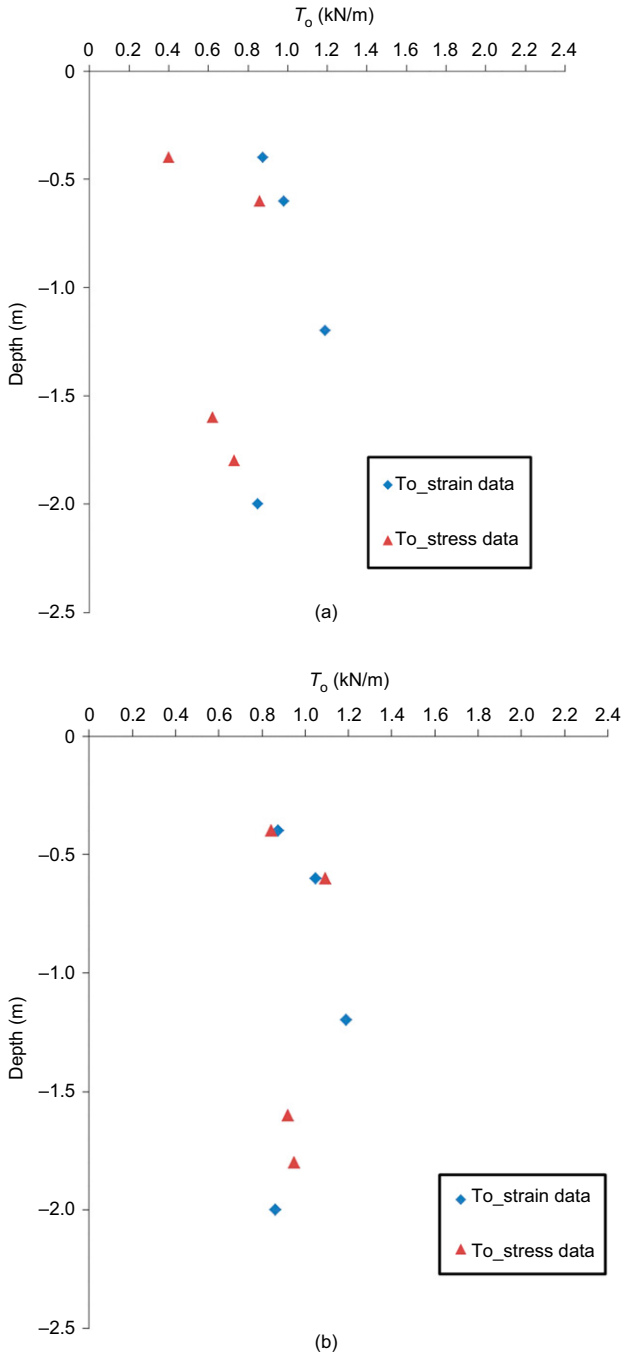

Figure 9. Comparison of connection load (T_o) distribution with depth after the placement of the slab estimated from two different approaches: (a) self-weight load; and (b) self-weight and slab load

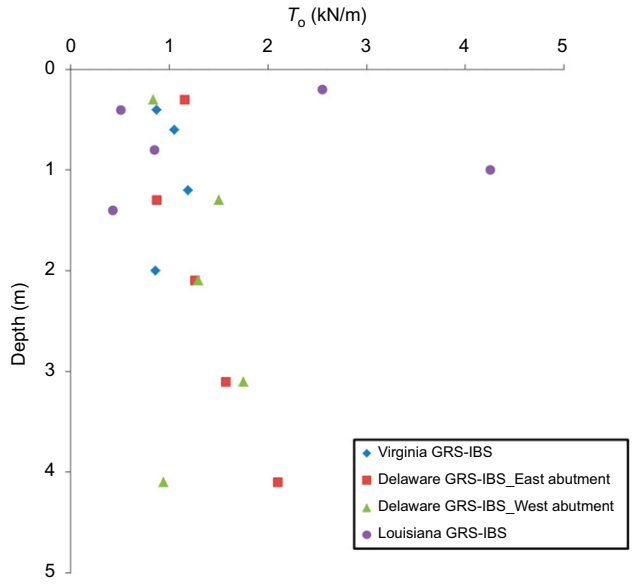

Figure 10. Comparison of connection load (T_o) distribution with depth due to self-weight and slab load estimated from three different GRS-IBS sites

The distribution of T_o with depth observed from approaches 1 and 2 showed a reasonably uniform distribution, not a triangular distribution as reported in Berg *et al.* (2009) or a bi-linear distribution as reported in Allen and Bathurst (2015, 2018). Further discussion on the distribution of T_o with depth is provided in the subsequent section.

5.4. Evaluation of T_o from other field monitoring GRS-IBS projects

The GRS-IBS constructed as part of this study presented an opportunity to conduct a comprehensive evaluation of T_o profiles with depth estimated using two different field data sources. To put into perspective the data presented herein, the T_o values obtained in this study were also compared to the T_o values estimated from two other projects located in Delaware and Louisiana. These comparisons were conducted using only the T_o values estimated based on the data obtained from SGs after placement of the slab (i.e. the data shown in Figure 7 for the Virginia GRS-IBS).

The GRS-IBS site in Delaware is located in New Castle County along Chesapeake City Road over the Guthrie Run stream. This site was selected for comparison because the aggregate (i.e. AASHTO No. 8), woven geotextile (i.e. having an ultimate tensile strength of 70 kN/m and a geotextile stiffness at 2% strain of 700 kN/m), and reinforcement vertical spacing (i.e. 0.2 m in the primary reinforcement zone) are very similar to the parameters used for construction of the Virginia GRS-IBS. Project-specific information for this site is provided by Meehan *et al.* (2016). The abutment constructed at this site has a height of 4.8 m (with a bearing bed 1 m in height) and a bridge span of 14.6 m. The unit weight of the AASHTO No. 8 aggregate was reported as 20 kN/m^3 and the friction angle was reported as 40°. The site was instrumented with short and long foil SGs placed alongside one another and glued to the geotextile at a horizontal distance of 0.25 m from the facing. The SGs were installed at depths of 0.3 m, 1.3 m, 2.1 m, 3.1 m, and 4.1 m below the superstructure on both abutments, which were designated east and west. T_o values for this site were calculated using Equation (4) and the average strain values obtained from the short and long foil strain gauges. Figure 10 depicts the results of calculated T_o values corresponding to both abutments. The results indicate that the magnitudes of T_o for the east abutment ranged from 0.8 to 2.1 kN/m and from 0.8 to 1.8 kN/m for the west abutment.

The GRS-IBS site in Louisiana is located on Route LA 91, close to Vermilion Parish. This site was also selected for comparison because the vertical spacing between reinforcements (i.e. 0.2 m within the primary reinforcement zone) is consistent with that in the Virginia GRS-IBS. Project-specific information for this site is provided by Saghebfar *et al.* (2016). The abutment constructed at this site has a height of 4.3 m (with a bearing bed 1 m in height) and a bridge span of 22 m. The aggregate used at the site classifies as open-graded crushed rock with a maximum particle size of 12.7 mm, a unit weight of 22.1 kN/m^3, and friction angle of 50.9° based on direct shear tests. The woven geotextile used at the site has an ultimate tensile strength of 80 kN/m and a stiffness at 2% strain of 850 kN/m. The site was instrumented with SGs located at a horizontal distance of 0.2 m from the facing and installed at depths of 0.2 m, 0.4 m, 0.8 m, 1 m, and 1.4 m below the superstructure. T_o values for this site, shown in Figure 10, were estimated following the same approach as that adopted for the Delaware and Virginia GRS-IBS. The results show that T_o values range from 0.4 to 4.3 kN/m.

When all T_o values estimated from the Virginia, Delaware (both abutments) and Louisiana sites are compared, the results showed that the T_o values for the Virginia and Delaware sites compare well and that the distribution of T_o with depth at both sites could be interpreted as relatively uniform. With the exception of T_o values obtained at depths of 0.2 and 1 m, the T_o values from the Louisiana GRS-IBS are also close to T_o values from the other projects. Overall, the T_o values obtained for all three sites range from 0.4 to 4.3 kN/m, which provides evidence of the existence of connection loads in GRS-IBS structures under service conditions.

6. IMPLICATIONS IN DESIGN

Berg *et al.* (2009) provides a diagram describing the relationship between the type of reinforcement and coefficient of lateral stress ratio used in the design of MSE structures. This relationship was developed based on a back analysis of the lateral stress ratio (K_r) from tensile stresses measured in the field via instrumentation and is a result of normalized data with respect to the Rankine lateral earth pressure coefficient (K_a). In this relationship, the K_r/K_a ratio for MSE structures reinforced with geosynthetics (extensible) is defined as constant with depth.

An approach similar to the AASHTO diagram was adopted to normalize the T_o data presented in this study from the Virginia, Delaware, and Louisiana GRS-IBS sites (Figure 10). The T_o data was converted to a lateral stress ratio (K_r) defined as follows

$$K_r = \frac{T_o}{(\sigma_v \times S_v)} \tag{6}$$

where K_r is the lateral stress ratio, T_o is the connection load estimated from geotextile strain data, σ_v is the vertical stress at a given depth after placement of the slab, and S_v is the vertical spacing between reinforcements.

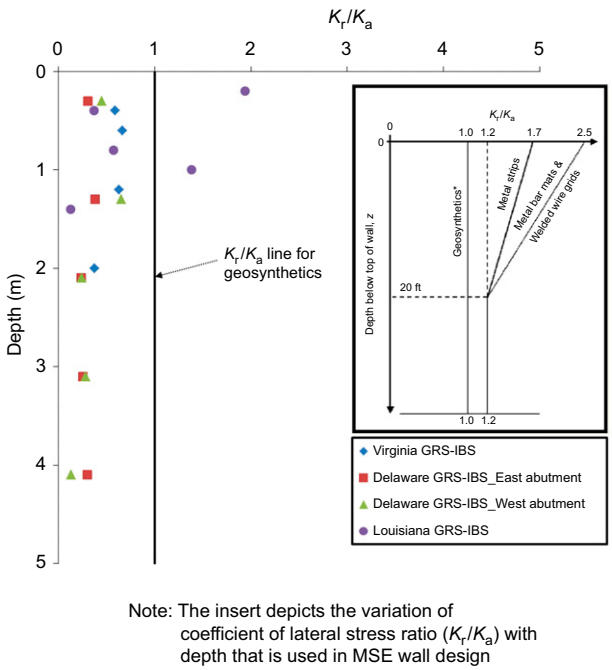

Note: The insert depicts the variation of coefficient of lateral stress ratio (K_r/K_a) with depth that is used in MSE wall design

Figure 11. Normalized connection load (T_o) distribution with depth from three different GRS-IBS sites. Note: The insert depicts the variation of coefficient of lateral stress ratio (K_r/K_a) with depth that is used in MSE wall design

Figure 11 shows the distribution of normalized T_o for all three sites evaluated in this study. A typical profile adopted for the coefficient of lateral stress ratio (K_r/K_a) with depth in the design of MSE structures reinforced with extensible and inextensible reinforcements is inserted into Figure 11 for comparison. The K_a for this estimation was calculated using Equation (2) based on the friction angle of the backfill reported for each site. The results in Figure 11 indicate that with the exception of the two points from the Louisiana site, all data from the three sites lie below the K_r/K_a line for geosynthetics as determined for MSE structures. This denotes that the theoretical approach outlined to estimate T_o as a function of lateral earth pressure and vertical reinforcement spacing in the design of MSE structures can conservatively be adopted to estimate T_o in GRS-IBS design.

7. CONCLUSIONS

This research aimed at evaluating the connection load in GRS-IBS structures under service loads based on the data obtained from field monitored GRS-IBS sites as well as at assessing the implications of these results for the existing design guidelines. In addition, the performance of a GRS-IBS constructed as part of this study was monitored to evaluate lateral stresses, reinforcement strains, and vertical and lateral deformations of the bridge. The findings from this study are presented as follows.

(1) The lateral stress distribution obtained from the field due to self-weight of backfill did not follow the triangular stress distribution predicted by the

theoretical earth pressure methods. The lateral stress distribution followed a reasonably uniform trend similar to the stress distribution trend assumed in the bin pressure method (Wu 2001; Adams *et al.* 2011; Adams and Nicks 2018). However, the magnitudes of stresses from the field were much higher than the stresses from the bin pressure method. The magnitudes of the lateral stresses from the field after applying the slab load were close to the stresses predicted by the active condition, and the stress distribution was found to be reasonably uniform.

(2) Reinforcement strains obtained from field measurements were smaller than 0.3%, which is significantly below the maximum allowable geosynthetic strains (2%) in GRS-IBS design (Adams *et al.* 2011; Adams and Nicks 2018). The strain distribution with depth in GRS-IBS is interpreted as uniform.

(3) Vertical deformation (settlement) of the foundation and lateral facing deformations of the GRS-IBS constructed in this study were observed as less than 5 mm. Both values are below the threshold outlined in the design of GRS-IBS (Adams *et al.* 2011; Adams and Nicks 2018).

(4) Connection load (T_o) values estimated using reinforcement strains and lateral stresses right behind the facing were in agreement, both in terms of distribution with depth and magnitude, which ranged from 0.8 to 1.2 kN/m.

(5) The magnitudes and distribution of T_o observed at two other sites were comparable with the T_o observed at the Virginia GRS-IBS. Overall, the T_o values observed for all projects was in the range of 0.4 to 4.3 kN/m. This indicates that connection loads developed in GRS-IBS structures require quantification as part of an internal stability analysis conducted as part of the design of these structures. However, the measured T_o values were found to be particularly small, and should be easily satisfied in terms of connection strength.

(6) The results of normalized T_o values from all three sites evaluated in this study confirmed that the theoretical approach to estimate T_o as function of the lateral earth pressure and vertical reinforcement spacing outlined in the design of MSE structures can conservatively be used to estimate T_o in the design of GRS-IBS.

ACKNOWLEDGEMENTS

This research was funded by the National Cooperative Highway Research Program (NCHRP) and the Virginia Department of Transportation (VDOT). Staunton District of VDOT has designed and constructed the GRS-IBS cited in this research. The authors would like to extend great appreciation to the individuals at the Virginia Center for Transportation Innovation and Research (VCTIR) and VDOT, especially M. Brown, R. Pearce, C. Weaver, J. Eulogio, I. Kim, J. Calhoun, and J. Uhl. The authors would also like to thank R. Drefus at Geocomp for his support in field instrumentation data collection systems and M. Vessely at Shannon and Wilson for providing access to the Colorado MSE bridge abutment instrumentation data. A. Abbaspour, S. Ullah, A. Morsy, and Y. Jiang are acknowledged for their generous help in the field during their graduate studies.

NOTATION

Basic SI units are shown in parentheses.

J	modulus of geotextile (N/m)
K_a	active lateral earth pressure coefficient (dimensionless)
K_o	at-rest lateral earth pressure coefficient (dimensionless)
K_r	lateral stress ratio (dimensionless)
K_r/K_a	coefficient of lateral stress ratio (dimensionless)
S_v	vertical reinforcement spacing (m)
T_{max}	maximum tension in reinforcement (N/m)
T_o	connection load (N/m)
Z	depth at a given stress point (m)
γ	unit weight of the backfill material (N/m^3)
$\Delta\sigma_V$	distributed vertical stress (N/m^2)
ε	geotextile strain (dimensionless)
σ_H	lateral earth pressure (N/m^2)
σ_v	vertical stress (N/m^2)
ϕ	friction angle of backfill (degrees)

ABBREVIATIONS

AASHTO	American Association of State Highway and Transportation Officials
CMU	concrete masonry unit
FHWA	Federal Highway Administration
GRS	geosynthetic reinforced soil
GRS-IBS	geosynthetic reinforced soil-integrated bridge system
MSE	mechanically stabilized earth
RPC	rectangular pressure cell
RSF	reinforced soil foundation
SC	settlement cell
SG	strain gage
ST	survey target
VDOT	Virginia Department of Transportation

REFERENCES

AASHTO (2020). *LRFD Bridge Design Specifications*, 9th edn. American Association of State Highway and Transportation Officials, Washington, DC, 1912p.

Abu-Hejleh, N., Zornberg, J. G., Elias, V. & Watcharamonthein, J. (2003). Design assessment of the Founders/Meadows GRS abutment structure. *Proceedings of Annual Meeting*, Transportation

Research Board, Washington, DC, USA, https://books.google.com/books/about/Transportation_Research_Board_82nd_Annua.html?id=1QL_jwEACAAJ (CD-ROM).

Adams, M. T. & Nicks, J. E. (2018). *Design and Construction Guidelines for Geosynthetic Reinforced Soil Abutments and Integrated Bridge Systems*, FHWA-HRT-17-080. Federal Highway Administration, McLean, VA, USA.

Adams, M. T., Nicks, J. E., Stabile, T., Wu, J. T. H., Schlatter, W. & Hartmann, J. (2011). *Geosynthetic Reinforced Soil Integrated Bridge System, Synthesis Report*, Report No. FHWA-HRT-11-027. Federal Highway Administration, McLean, VA, USA.

Allen, T. M. & Bathurst, R. J. (2002). Soil reinforcement loads in geosynthetic walls at working stress conditions. *Geosynthetics International*, **9**, No. 5–6, 525–566.

Allen, T. M. & Bathurst, R. J. (2015). An improved simplified method for prediction of loads in reinforced soil walls. *ASCE Journal of Geotechnical and Geoenvironmental Engineering*, **141**, No. 11, 04015049.

Allen, T. M. & Bathurst, R. J. (2018). Application of the simplified stiffness method to design of reinforced soil walls. *ASCE Journal of Geotechnical and Geoenvironmental Engineering*, **144**, No. 5, 04018024.

Allen, T. M. & Bathurst, R. J. (2019). Geosynthetic reinforcement stiffness characterization for MSE wall design. *Geosynthetics International*, **26**, No. 6, 592–610.

Ardah, A., Abu-Farsakh, M. & Voyiadjis, G. Z. (2018). Numerical evaluation of the effect of differential settlement on the performance of GRS-IBS. *Geosynthetics International*, **26**, No. 4, 427–441.

Awad, M. I. & Tanyu, B. F. (2014). Laboratory evaluation of governing mechanism of frictionally connected MSEW face and implications on design. *Geotextiles and Geomembranes*, **42**, No. 5, 468–478.

Bathurst, R. J., Allen, T. M. & Walters, D. L. (2005). Reinforcement loads in geosynthetic walls and the case for a new working stress design method. *Geotextiles and Geomembranes*, **23**, No. 4, 287–322.

Berg, R. R., Christopher, B. R. & Samtani, N. C. (2009). *Design and Construction of Mechanically Stabilized Earth Walls and Reinforced Soil Slopes*, FHWA NHI-10-024 Vol I and NHI-10-025 Vol II, U.S. DOTFHWA-NHI-09-083 and FHWA GEC-011. Federal Highway Administration, Washington, DC, USA, pp. 306 (Vol I) and pp. 378 (Vol II).

Bloser, S., Shearer, D., Corradini, K. & Scheetz, B. (2012). *Geosynthetically Reinforced Soil-Integrated Bridge Systems (GRS-IBS) Specification Development for PennDOT Publication 447*. Publication No. 447 (10-14), Pennsylvania Department of Transportation, PA, USA.

Budge, A., Dasenbrock, D., Mattison, D., Bryant, G., Grosser, A., Adams, M. & Nicks, J. (2014). Instrumentation and early performance of a large grade GRS-IBS wall. *Geo-Congress 2014 Technical Papers. Geo-Characterization and Modeling for Sustainability*, Abu-Farsakh, M., Yu, X. & Hoyos, L. R. Editors, ASCE, Reston, VA, USA.

Christopher, B. R. (1993). *Deformation Response and Wall Stiffness in Relation to Reinforced Soil Wall Design*. Ph.D. Dissertation, Department of Civil EngineeringPurdue University, West Lafayette, IN, USA, 354p.

Christopher, B. R., Gill, S. A., Giroud, J. P., Juran, I., Scholsser, F., Mitchell, J. K. & Dunnicliff, J. (1989). *Reinforced Soil Structures, Volume I. Design and Construction Guidelines*, Report No. FHWA-RD-89-043. U.S. Department of Transportation, Federal Highway Administration, Washington, DC, USA, 287p.

Gebremariam, F., Tanyu, B. F., Christopher, B., Leschinsky, D., Han, J. & Zornberg, J. G. (2020). Evaluation of vertical stress distribution in field monitored GRS-IBS structure. *Geosynthetics International*, https://doi.org/10.1680/jgein.20.00004.

Jaky, J. (1948). Pressure in silos. *2nd ICSMFE, London*, **1**, 103–107.

Jiang, Y., Han, J., Parsons, R. L. & Cai, H. (2015). *Field Monitoring of MSE Walls to Investigate Secondary Reinforcement Effects, Report*. The Kansas Department of Transportation, Kansas, KS, USA.

Ling, P. & Leshchinsky, D. (1996). *Mesa Walls: Field Data Reduction, Finite Element Analysis, and Preliminary Design Recommendations, Report*. Tensar Earth Technologies, Inc., Atlanta, GA, USA.

Meehan, F., Talebi, M. & Poggiogalle, B. (2016). *Analysis of the Field Behavior of A Geosynthetic Reinforced Soil Integrated Bridge System During Construction and Operation*, Report No. DC2 262. Delaware Center of Transportation, Newark, DE, USA.

Morrison, K. F., Harrison, F. E., Collin, J. G., Dodds, A. & Arndt, B. (2006). *Shored Mechanically Stabilized Earth (SMSE) Wall Systems Design Guidelines*, Report No. FHWA-CFL/TD-06-001. Federal Highway Administration, McLean, VA, USA.

Nicks, J. E. & Adams, M. T. (2019). Lateral earth pressure distribution with depth for GRS mini-abutments. *Proceedings of the Geosynthetics Conference, Houston, TX, USA*, https://geosyntheticsconference.com/proceedings-archive/.

Nicks, J. E., Adams, M. T. & Stabile, T. (2013). Performance testing for geosynthetic reinforced soil composites. *Proceedings of the 5th International Young Geotechnical Engineers' Conference, Marne-la-Vallée, France*, Cui, Y.-J., Emeriault, F., Cuira, F., Ghabezloo, S., Pereira, J.-M., Reboul, M., Ravel, H. & Tang, A. M. Editors.

Saghebfar, M., Abu-Farsakh, M., Ardah, A., Chen, Q. & Fernandez, B. A. (2016). Performance monitoring of geosynthetic reinforced soil integrated bridge system (GRS-IBS) in Louisiana. *Geotextiles and Geomembranes*, **45**, No. 2017, 34–47.

Stulgis, R. P. (2006). Full-scale MSE test walls. GeoTesting Express, Inc., Boxborough, MA, USA.

Tencate Geosynthetics (2015). Specification sheet for Mirafi HP570 geotextile. See https://www.tencategeo.us/media/6a00f4f6-483f-4e7d-a5b4-27a79ded079b/306CSw/TenCate%20Geosynthetics/Documents%20AMER/Technical%20Data%20Sheets/Woven/Mirafi%20HP-Series/TDS_HP570A.pdf (accessed 25/04/2019).

Warren, K. A., Whelan, M. J., Hite, J. & Adams, M. (2014). Three-year evaluation of thermally induced strain and corresponding lateral end pressures for a GRS IBS in Ohio. In *Proceedings, Geo-Congress 2014. Geo-Characterization and Modeling for Sustainability*, Atlanta, GA. ASCE, Reston, VA, USA, pp. 4238-4251.

Wu, J. T. H. (2001). *Revising the AASHTO Guidelines for Design and Construction of GRS Walls*, Report No. CDOT-DTD-R-2001-16. Colorado Department of Transportation, Denver, CO, USA.

Wu, J. T. H., Ketchart, K. & Adams, M. T. (2001). *GRS Piers and Abutments*, Report No. FHWA-RD-00-038. Federal Highway Administration, McLean, VA, USA.

Zornberg, J. G., Morsy, A. M. & Mofarraj, B., Christopher, B. R., Leshchinsky, D., Han, J., Tanyu, B. F., Gebremariam, F. T., Shen, P. & Jiang, Y. (2018). *Defining the Boundary Conditions for Composite Behavior of Geosynthetic Reinforced Soil (GRS) Structures*, National Cooperative Highway Research Program (NCHRP), Project 24-41. Transportation Research Board, Washington, DC, USA, October, 986p.

Zornberg, J. G., Morsy, A. M., Mofarraj, B., Christopher, B. R., Leshchinsky, D., Han, J., Tanyu, B. F., Gebremariam, F. T., Shen, P. & Jiang, Y. (2019). *Proposed Refinements to Design Procedures for Geosynthetic Reinforced Soil (GRS) Structures in AASHTO LRFD Bridge Design Specifications*, National Cooperative Highway Research Program (NCHRP), Project 24-41. Transportation Research Board, Washington, DC, USA, March, 64p.

The Editor welcomes discussion on all papers published in Geosynthetics International. Please email your contribution to discussion@geosynthetics-international.com by 15 June 2021.